energies

MDPI

Article

Traction Load Modeling and Parameter Identification Based on Improved Sparrow Search Algorithm

Zhensheng Wu [1], Deling Fan [1,*] and Fan Zou [2]

[1] School of Electrical Engineering, Beijing Jiaotong University, Beijing 100044, China; zhshwu@bjtu.edu.cn
[2] Department of Earth Science, Uppsala University, 62157 Visby, Sweden; fan.zou@geo.uu.se
* Correspondence: 20121429@bjtu.edu.cn; Tel.: +86-188-0010-9417

Abstract: In this paper, a traction load model parameter identification method based on the improved sparrow search algorithm (ISSA) is proposed. According to the load characteristics of the AC traction power supply system under transient disturbance, the model structure of the traction load is equated to the composite load model structure of the static load shunt induction motor's dynamic load. The traditional sparrow search algorithm is improved to enhance its accuracy and convergence. The generalization ability of the model was tested, and the accuracy of the proposed model was verified. Using the ISSA to determine the load model from the measured data, the results can verify the effectiveness of the ISSA for comprehensive load model parameter identification. Comparing the ISSA with the traditional SSA and PSO algorithms, it shows that the ISSA has better accuracy and convergence.

Keywords: improved sparrow search algorithm; parameter identification; traction load; load modeling

Citation: Wu, Z.; Fan, D.; Zou, F. Traction Load Modeling and Parameter Identification Based on Improved Sparrow Search Algorithm. *Energies* **2022**, *15*, 5034. https://doi.org/10.3390/en15145034

Academic Editor: Surender Reddy Salkuti

Received: 18 June 2022
Accepted: 7 July 2022
Published: 10 July 2022

1. Introduction

Power systems consist of three main components: the generating unit, the transmission network, and the electrical load. With the continuous updating of computer technology, digital simulation of power systems [1] has become an important tool for power system planning, design, and computational analysis at present. The accuracy of the power system model required for simulation has attracted increasing attention from scholars. So far, the modeling studies of generators and transmission networks are quite mature with the continuous efforts of scholars. Compared with other components, the modeling of electric loads is still very difficult because of the variety of loads. The complex composition, complexity of dynamic and static characteristics, and other factors all lead to randomness, dispersion, and time-varying nature of loads. A large number of experiments and actual operating conditions of power systems already show that the load model has an important influence on the tide calculation, voltage stability analysis, and transient stability analysis of power systems. The establishment of a suitable and accurate load model is of great significance for the digital simulation of power systems.

Traction loads are characterized by randomness, asymmetry, and low power factor. The problems of power quality, such as harmonics and negative sequence currents of traction loads, are not the main focus of transient stability studies; the study of their transient characteristics mainly depends on the performance of the system after its dynamic characteristics are changed by transient disturbances [2,3]. Thus, an accurate traction load equivalent composite load model should be established, and its transient stability could be studied by means of professional power system transient simulation analysis.

Currently, load modeling methods include statistical synthesis [4], overall measurement and identification [5], and fault simulation [6]. The basic idea of the overall measurement and identification method is to treat the load as a whole system, first determining the load model structure and then using the data collected in the field and the effective identification algorithm to identify the relevant parameters of the load model structure, check the

accuracy of the model, and then output the load model after the error meets the accuracy requirements [7]. The overall measurement and identification method is an effective way to solve complex integrated load modeling without the need to understand the complex composition within the load. Parameter identification is the core of this method, and the evolving system identification theory provides a strong theoretical basis for this method. Therefore, choosing a suitable parameter identification method is the key to the accuracy of load modeling.

Load model parameter identification can be divided into linear and nonlinear methods. Linear methods mainly include the least squares method, Kalman filter method [8], etc. The nonlinear parameter identification method is mainly based on the optimization algorithm, and the main idea is to find a set of optimal parameter solutions to minimize the preset objective function. At present, the main nonlinear methods proposed are the gradient method, random search method, and simulated evolution method. In [9], a genetic algorithm is first introduced into the parameter identification of the induction motor load model. In [10], a genetic algorithm (GA) and the Levenberg–Marquardt (L–M) algorithm are combined to identify parameters of the comprehensive load model, which improves the accuracy and efficiency of identification. In [11], a combination of chaos and quantum particle swarm algorithms was used to carry out the parameter identification of the integrated load model, and it indicated that the CQDPSO algorithm has better performance in terms of convergence speed and accuracy.

In recent years, many scholars have proposed many new intelligent optimization algorithms [12–15] by analyzing different biological populations and physical phenomena. The sparrow search algorithm is a new group intelligence algorithm proposed by scholar Xue [16] in 2020, and it has been widely used by scholars because of its excellent convergence and accuracy. Scholar Li [17] tested the typical swarm intelligence algorithms proposed in recent years and compared the experimental performance of these algorithms in terms of convergence speed, accuracy, and stability through 22 standard CEC test functions; the results show that the sparrow search algorithm has better convergence, accuracy, and variance. However, it is still easy to converge prematurely and fall into a local optimum when solving complex nonlinear problems. Therefore, it is necessary to optimize its existing algorithm process to improve the algorithm accuracy and convergence performance. In [18], the authors introduced the random walk strategy into the SSA, proposed an adaptive sparrow search algorithm, and applied it to the model parameter optimization identification of proton exchange membrane fuel cell stack. The results show that the proposed algorithm has the best efficiency compared with the comparison algorithm. In [19], the improved sparrow search algorithm is applied to the IEEE33 nodes of the distributed-generation optimization configuration model, and the DG configuration scheme can reduce the active power loss and voltage deviation of the distribution network to a greater extent. In [20], the population is initialized by using the barycenter reversal mechanism. Aiming at the shortage of the global search ability of the discoverer, the learning coefficient is introduced into the position update part, and the improved algorithm is applied to the photovoltaic microgrid system. The results show that compared with the comparison algorithm, the algorithm can track the maximum power point more accurately with good robustness. However, the paper only used the particle swarm optimization algorithm for comparative experiments, and there is no benchmark function experiment based on it, which cannot fully explain the universality of the improvement strategy. In [21], an improved sparrow search algorithm is proposed by combining the sparrow search algorithm with the UAV planning problem. The convergence speed and detection ability of the adaptive inertia weight balance algorithm are adopted, and the Cauchy–Gaussian mutation strategy is introduced to improve the anti-stagnation ability of the algorithm. The experimental results show that the algorithm can more effectively solve the UAV route planning problem. In [22], the Kent chaos mapping, Student-t distribution, and Lévy flight strategy are combined with the basic sparrow search algorithm and applied to the unknown load robotic arm parameter identification.

In order to verify the application effectiveness of the power system load parameter identification method combined with the SSA, we proposed an improved sparrow search algorithm by adding tent chaos mapping, Levy flight strategy, Gaussian perturbation after population update, and tent chaos perturbation on the basis of the conventional sparrow search algorithm. In order to verify the performance of the algorithm, the paper performs parameter identification of the proposed traction load model. The method is compared with the conventional sparrow search algorithm and particle swarm optimization (PSO) algorithm. After satisfying the error accuracy, we check the generalization ability of the identified load model. The article verifies the practicality of the ISSA to solve the optimization problem of load modeling parameter identification.

2. Modeling the Load

The main power component of the traction power supply system of the electrified railroad is the high-power traction motor on the traction locomotive, which is a three-phase asynchronous motor by nature and has obvious dynamic load characteristics. In addition, there are many small power components including air conditioning, lighting, and other static loads. Therefore, based on the load characteristics, the traction side can be equated to a composite load model with a parallel static load of motors when viewed from the grid side to the traction side, as in Figure 1. The load model uses a third-order induction motor dynamic load model in parallel with an exponential static load model [23].

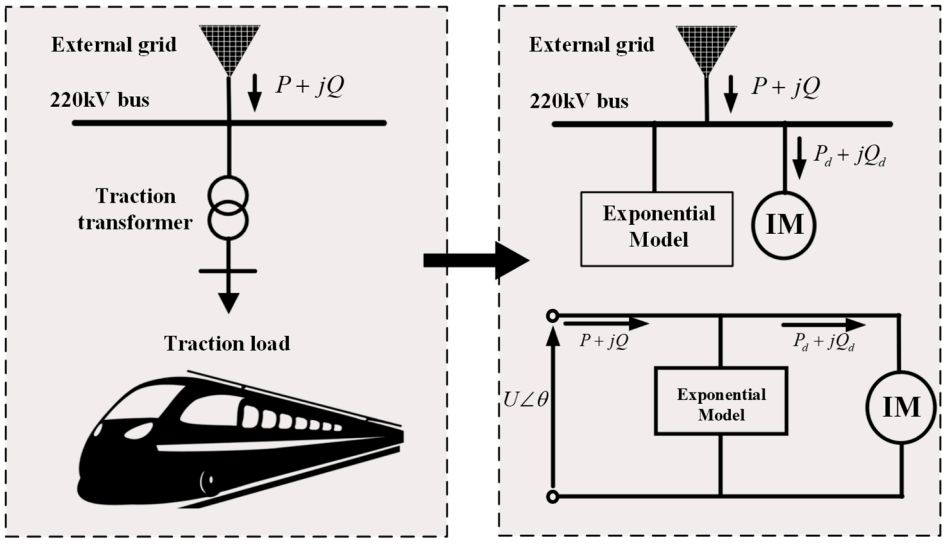

Figure 1. Traction composite load equivalence model.

According to the research of previous scholars, induction motor transient models [24,25] are usually divided into electromechanical transient models, mechanical transient models, and voltage transient models according to the different amounts of parameters, such as dynamic response accuracy of active power and voltage stability index accuracy. A comparison of these three motor models is presented in Table 1.

Among the many models proposed above, the third electromechanical transient model is generally suitable for the induction motor transient analysis problem, considering the balance of calculation volume and calculation accuracy. Since the work of this paper mainly focuses on the active power response and reactive power response of the load after the transient voltage disturbance, the dynamic load part of this paper adopts the third induction motor electromechanical transient model, and the static load is described by the exponential static model with few parameters and acceptable accuracy. It is shown schematically in Figure 2.

Table 1. Comparison of three induction motor models.

Induction Motor Model	Active Power Response Accuracy	Reactive Power Response Accuracy	Stability Accuracy	Parameter Identifiability	Calculation Size
Electromechanical transient model	Better	Better	Better	Identifiable	Large
Mechanical transient model	Good	Bad	Better	Unidentifiable	Small
Voltage transient model	Bad	Good	Good	Unidentifiable	Small

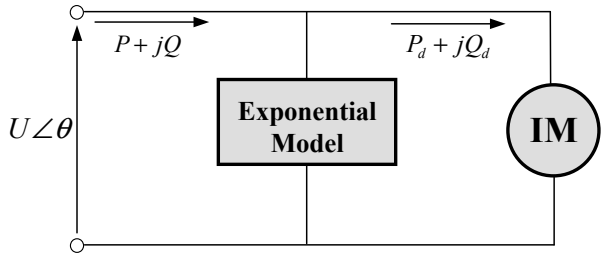

Figure 2. A schematic of the exponential-induction motor model.

2.1. Dynamic Load Section

In order to increase the calculation accuracy and the calculation volume, and also reduce the number of parameters to be identified, the third model of induction motor adopts the polar coordinate form [26], and its state equation and power output equation are as shown in Equations (1) and (2).

- Equation of state.

$$\begin{cases} T'\frac{dE'}{dt} = -E' + CU\cos\delta \\ \frac{d\delta}{dt} = -\frac{CU\sin\delta}{T'E'} + \omega - \omega_s \\ M\frac{d\omega}{dt} = -\frac{UE'\sin\delta}{X'} - T_m \end{cases} \tag{1}$$

- Power output equation.

$$\begin{cases} P_d = -\frac{UE'}{X'}\sin\delta \\ Q_d = \frac{U(U-E'\cos\delta)}{X'} \end{cases} \tag{2}$$

In Equation (2), $E' = \sqrt{E'^2_d + E'^2_q}$, $\delta = \arctan(-\frac{E_d{}'}{E_q{}'})$, $C = \frac{X-X'}{X}$, and $T' = \frac{X'}{X}T'_0$, where E' is the induction electric potential amplitude, δ is the angle behind transient reactance, ω_S is the angular velocity of stator, ω_r is the angular velocity of rotor, X_m is the magnetizing reactance, X_s is the rotor reactance, X_r is the rotor reactance,$X' = X_s + X_m X_r/(X_m + X_r)$ is the transient reactance, $X = X_m + X_s$ is the open-circuit reactance, $T_0{}' = (X_m + X_r)/(\omega_s R_r)$ is the rotor open-circuit time constant, R_r is the rotor resistance (zero stator resistance is assumed), M is the motor inertia, T_m is the load torque constant, and P_d and Q_d are the dynamic load active and reactive power, respectively.

In Equation (1), E', δ, ω are the state variables. Since the differential of the state quantity is 0 in the steady-state process, it can be determined that the initial value of the state variable is solved as shown in Equation (3) as follows:

$$\begin{cases} \delta_0 = \frac{1}{2}\arcsin(-\frac{2T_m X'}{CU_0{}^2}) \\ E_0{}' = CU_0\cos\delta_0 \\ \omega_0 = \omega_s + \frac{CU_0\sin\delta_0}{T'E_0{}'} \end{cases} \tag{3}$$

In the iterative process of solving the optimal parameters of the load model, each iteration involves the calculation of the dynamic process of dynamic load state quantities. In this paper, the state differential equation is solved using the fourth-order Runge–Kutta methods in the iterative process. The principle of the formulation is described in Equation (4) as follows:

$$\begin{cases} y_{n+1} = y_n + \frac{h}{6}(K_1 + 2K_2 + 2K_3 + K_4) \\ K_1 = f(x_n, y_n) \\ K_2 = f(x_n + \frac{h}{2}, y_n + \frac{h}{6}K_1) \\ K_1 = f(x_n + \frac{h}{2}, y_n + \frac{h}{6}K_2) \\ K_1 = f(x_n + h, y_n + hK_3) \end{cases} \tag{4}$$

After solving the equation of state by the fourth-order Runge–Kutta methods, the state variable iteration equation can be obtained as:

$$\begin{bmatrix} E'_{n+1} \\ \delta_{n+1} \\ \omega_{n+1} \end{bmatrix} = \begin{bmatrix} E'_n \\ \delta_n \\ \omega_n \end{bmatrix} + \frac{h}{6}\left(\begin{bmatrix} K_{11} \\ K_{12} \\ K_{13} \end{bmatrix} + 2\begin{bmatrix} K_{21} \\ K_{22} \\ K_{23} \end{bmatrix} + 2\begin{bmatrix} K_{31} \\ K_{32} \\ K_{33} \end{bmatrix} + \begin{bmatrix} K_{41} \\ K_{42} \\ K_{43} \end{bmatrix} \right) \tag{5}$$

Therefore, the above Equation (5) and the state variable initial value of Equation (3) can be combined to iteratively calculate the induction motor in the time domain.

2.2. Static Load Section

The exponential function load model is chosen for the static part, ignoring the variation of frequency, and its expression is described as follows:

$$\begin{cases} P_s = P_{s0}(\frac{U}{U_0})^{p_v} \\ Q_s = Q_{s0}(\frac{U}{U_0})^{q_v} \end{cases} \tag{6}$$

where P_s, Q_s are the active and reactive power of the static load, respectively, P_{s0}, Q_{s0} are the active power and reactive power of the steady state before the disturbance, respectively, U_0 is the steady-state voltage, and p_v, q_v are the active power index and reactive power index, respectively.

2.3. Parameter Identification

From the above two subsections, the total power absorbed by the composite load is shown in Equation (7) as follows:

$$\begin{cases} P = P_s + P_d = P_{s0}(\frac{U}{U_0})^{p_v} - \frac{UE'}{X'}\sin\delta \\ Q = Q_s + Q_d = Q_{s0}(\frac{U}{U_0})^{q_v} + \frac{U(U - E'\cos\delta)}{X'} \end{cases} \tag{7}$$

In summary, the parameters to be determined for this integrated load model consist of five dynamic load parameters $\theta_d = [T', X', C, M, T_m]$ and two static load parameters $\theta_s = [p_v, q_v]$, and the set of parameters identified is $\theta = [T', X', C, M, T_m, p_v, q_v]$.

The objective function of parameter identification is generally taken as a non-negative monotonic increasing function of the output error, the squared error sum of the measured response of the system, and the calculated response of the model is used as the objective function.

$$Obj.E(\theta) = \min\varepsilon^*(\theta) = \frac{1}{N}\min\sum_{k=1}^{N}\left[(P_k - \hat{P}_k)^2 + (Q_k - \hat{Q}_k)^2\right] \tag{8}$$

Here, P_k and Q_k are the measured active power and reactive power, $\hat{P}_k$ and $\hat{Q}_k$ are the model calculates the output active and reactive power, and N is the number of sample data sets.

3. Traditional Sparrow Search Algorithm and Its Improvement

3.1. Traditional Sparrow Search Algorithm

The sparrow search algorithm (SSA) is a new group intelligent optimization algorithms proposed by Xue [16] in 2020 to simulate sparrow population searching. The background and rationale of this algorithm are mainly based on the foraging and anti-predatory behaviors of sparrow populations. This algorithm enables sparrows within a population to update the positions of discoverers, joiners, and perceivers by continuously comparing fitness values until the optimal solution of the objective function is found.

The sparrow search algorithm is divided into three sparrow populations based on their characteristics and adaptability (energy contained in themselves), as described below:

- Producer: Producers are characterized by high fitness values and a wide search range, and they are responsible for finding food for the entire population and providing foraging directions;
- Scrounger: Scroungers have low fitness values, but they always watch the Producers and leave their current location to compete for food if they sense that the Producers have found better food;
- Perceiver: Perceivers originate from the Producers and the Scroungers. They can realize the update of the position by perceiving the danger.

The general content of the sparrow search algorithm is as follows. In the case of an optimization problem, the population composed of sparrows is as follows:

$$X = \begin{bmatrix} x_{1,1} & x_{1,2} & \cdots & x_{1,d} \\ x_{2,1} & x_{2,2} & \cdots & x_{2,d} \\ \vdots & \vdots & \vdots & \vdots \\ x_{n,1} & x_{n,2} & \cdots & x_{n,d} \end{bmatrix} \tag{9}$$

where d denotes the dimension of the parameter to be optimized for this problem, and n indicates the number of sparrows. It can be determined that the fitness value of the sparrow is expressed as follows:

$$fit(X) = \begin{bmatrix} f([x_{1,1}, x_{1,2}, \ldots, x_{1,d}]) \\ f([x_{2,1}, x_{2,2}, \ldots, x_{2,d}]) \\ \vdots \\ f([x_{n,1}, x_{n,2}, \ldots, x_{n,d}]) \end{bmatrix} \tag{10}$$

In the SSA, the location of the Producer is updated as described below:

$$X_{i,j}^{t+1} = \begin{cases} X_{i,j}^{t} \exp(-\frac{i}{\alpha iter_{Max}}) & if R_2 < ST \\ X_{i,j}^{t} + QL & if R_2 \geq ST \end{cases} \tag{11}$$

where t is the number of current iterations, j is the dimension of the parameters, $item_{Max}$ is the maximum number of iterations, $X_{i,j}$ is the position coordinate of the i sparrow in the j dimension, $\alpha \in (0, 1]$ is a random number, and $ST \in [0.5, 1]$ represent the alarm value and the safety threshold, respectively, Q represents a random number that obeys normal distribution, and L represents a matrix with one row and d columns, of which all its elements are 1. There are two situations about the location change of the Producers: when $R_2 < ST$, there are no predators around in this environment, and the Producers can carry out extensive search. When $R_2 \geq ST$, a sparrow in the population has spotted predators and sends a warning signal to other sparrows in the entire population, at which point all sparrows should immediately fly to other safe locations.

In the SSA, the location of the Scrounger is updated as described below:

$$X_{i,j}^{t+1} = \begin{cases} Q\exp(\frac{X_{worst}-X_{i,j}^{t}}{i^2}) & ifi > \frac{n}{2} \\ X_P^{t+1} + \left|X_{i,j}^{t} - X_p^{t+1}\right| A^+ L & otherwise \end{cases} \quad (12)$$

where X_P represents the best location discovered by the Producers, and represents the current global worst position. $A^+ = A^T(AA^T)^{-1}$, in which A represents a matrix with one row and d columns and where each element in the matrix is randomly assigned 1 or -1. When $i > n/2$, it means that the number i Scrounger with low fitness did not obtain food, so at this time it should change the position to obtain more energy.

In the SSA, for Perceivers who are aware of danger, we usually give 10–20% of the sparrows in the whole population. Its location update is described below.

$$X_{i,j}^{t+1} = \begin{cases} X_{best}^{t} + \beta\left|X_{i,j}^{t} - X_{best}^{t}\right| & if\ f_i > f_g \\ X_{i,j}^{t} + K\frac{\left|X_{i,j}^{t} - X_{worst}^{t}\right|}{(f_i - f_{wrost}) + \varepsilon} & if\ f_i = f_g \end{cases} \quad (13)$$

Here, X_{best} is the current global best position, and $\beta \sim N(0,1)$ is a random number that represents the step control parameter. $K \in [-1,1]$ represents the direction of sparrow movement, which is also a step size control parameter and a random number. f_i represents the fitness value of the current individual sparrow. ε represents an infinitesimal constant, which is used to avoid the occurrence of 0 in the denominator of the above formula. There are two situations for the position change of the perceiver. When $f_i > f_g$, the sparrow is at the edge of the population and easy to be attacked by predators. When $f_i = f_g$, it means that the sparrow in the middle of the population is aware of the danger and needs to move to the position of other sparrows to avoid the danger.

3.2. Improvement of Sparrow Search Algorithm

3.2.1. Tent Chaotic Mapping

This paper uses a tent chaotic map [27] to initialize the sparrow population. A chaotic system is a kind of seemingly disordered but complex and orderly non-random motion, which has the characteristics of randomness, ergodicity, and regularity. Common chaotic maps include a circle map and logistic map, etc. Tent mapping and logistic mapping are topologically conjugate. A related study [28] shows that a tent map has better ergodic uniformity than a logistic map through comparative experiments. Therefore, a tent map is selected as the chaotic map in this study. The iteration formula of tent mapping is as follows:

$$X_{t+1} = \begin{cases} \frac{X_t}{\alpha} & X \in [0,\alpha) \\ \frac{1-X_t}{1-\alpha} & X \in [\alpha,1] \end{cases} \quad (14)$$

where $\alpha \in (0,1)$, $X_n \in [0,1], n = 1,2,\ldots$.

In this study, by setting the parameters of three dimensions and performing tent chaotic mapping between (0,1), it is found that when 0.3 is taken, the variables have relatively good randomness, ergodicity, and regularity, and the iteration diagram of the tent mapping is as shown in Figure 3.

3.2.2. Lévy Flight Strategy

When the Scroungers notice that the Producers have searched for a large amount of food, they will flock to the new location together. This situation will easily cause the joiners to gather to a certain search area at the same time, which will cause the global search ability to decrease and even make the algorithm fall into a local optimum in serious cases. To solve the above problem, we introduce the random step size of Lévy flight [29] when the Scroungers update its position and use its step size s and the uncertainty of its direction to

enhance the search ability of the algorithm, avoiding premature convergence of the search and falling into a local optimum.

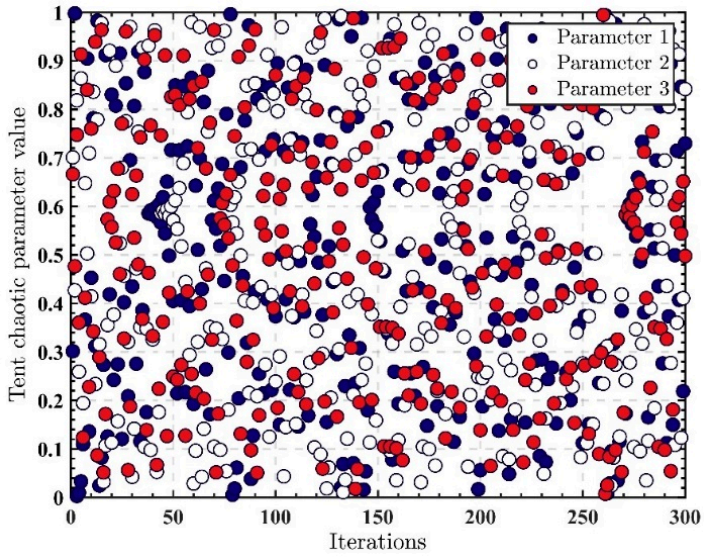

Figure 3. Schematic diagram of tent chaotic mapping.

The random step s size of the Lévy flight strategy is described as follows.

$$\begin{cases} s = \frac{\mu}{|\nu|^{\frac{1}{\beta}}}, \beta = 3/2 \\ \mu \sim N(0, \sigma_\mu^2) \\ \nu \sim N(0, \sigma_\nu^2) \\ \sigma_\mu = \left\{ \frac{\Gamma(1+\beta)\sin(\pi\beta/2)}{2^{(\beta-1)/2}\beta\Gamma[(1+\beta)/2]} \right\}^{\frac{1}{\beta}} \\ \sigma_\nu = 1 \end{cases} \tag{15}$$

The location update following the introduction of the Lévy flight strategy by the Scroungers is described as follows.

$$X_{i,j}^{t+1} = \begin{cases} Q\exp(\frac{X_{worst} - X_{i,j}^t}{i^2}) & if\ i > \frac{n}{2} \\ X_P^{t+1} + s \otimes \left| X_{i,j}^t - X_p^{t+1} \right| A^+ L & otherwise \end{cases} \tag{16}$$

We selected three sets of parameters for their Lévy flight iterations, and it can be seen from Figure 4 that each parameter has good randomness and uncertainty in its Lévy flight step and direction during the iterative process, realizing the diversity of population position changes.

3.2.3. Gaussian Variation and Tent Chaos Perturbation

Gaussian variation refers to a perturbation of the current global optimal solution searched for by a random number satisfying a Gaussian distribution during each iteration of the search for the optimal solution, which is described by the perturbation formula as follows:

$$X_{best}{}' = X_{best}(1 + N), \qquad N \sim N(0, 1) \tag{17}$$

where X_{best} represents the global optimal solution of the search at the current iteration number, and $X_{best}{}'$ represents the new value of the global optimum after Gaussian perturbation. From the Gaussian distribution properties, it is known that the introduction of Gaussian variation enhances the local search ability of the sparrow, which is conducive to inducing the population to jump out of the local optimal solution and find the global optimal solution.

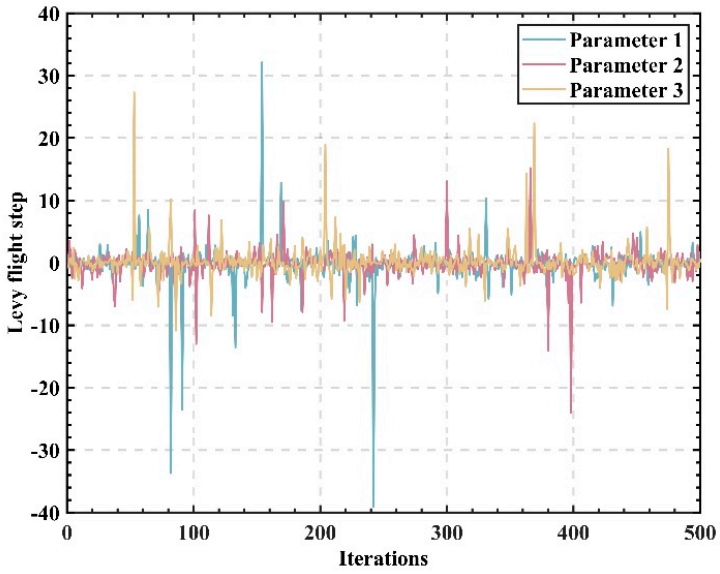

Figure 4. Lévy flight iterations.

The tent chaos perturbation is derived from the tent chaos mapping, which uses chaotic variables Z_d acting on parameter variables in d dimensions and is formulated as follows:

$$X_d = \min_d + (\max_d - \min_d) Z_d \tag{18}$$

where $\max_d$ and $\min_d$ are the maximum and minimum values of the d dimension parameters, respectively. The tent chaotic perturbation iterative update equation is described as follows:

$$X_{new}{}' = (X' + X)/2 \tag{19}$$

where X' represents the position of the individual sparrow to be disturbed, X is the generated perturbation variable, and $X_{new}{}'$ represents the position of an individual sparrow after chaotic perturbation.

According to the characteristics of Gaussian distribution, the main disturbance area of Gaussian disturbance is the local area near the original individual, which is conducive to the algorithm efficiently finding the minimum point of the current search area. Meanwhile, the tent chaotic disturbance can make the original individual have better randomness and ergodicity after disturbance, which can help the algorithm jump out of local optimization and prevent "premature". Therefore, this paper uses tent chaos perturbation in the early stage of algorithm optimization to search in a large range, which is as much as possible to avoid "premature", and it uses Gaussian perturbation to search in a small range more carefully in the late stage of optimization to speed up the convergence.

3.3. Improved Sparrow Search Algorithm Solving Process

According to the improvement of the algorithm in Section 3.2, the parameter identification process of the improved sparrow-based search algorithm in this study is implemented as follows:

- Step 1: set the number of groups of parameters to be identified (population size N), number of dimensions of parameters to be identified (dimensions d), number of Producers PD, number of Perceiver SD, safety threshold ST, maximum number of iterations $Iter_{\max}$, and the objective function $Obj.f(x)$;
- Step 2: apply tent chaos mapping to initialize the population location X_i and generate N d-dimensional sparrow individuals;
- Step 3: After setting the objective function $Obj.f(x)$, the current fitness value f_i is calculated for each individual sparrow (the objective function value is taken as the

fitness value in this study), and then the current optimal fitness value f_g and the current worst fitness value f_w are determined in order. Record the positions X_g and X_w corresponding to the fitness values;

- Step 4: Compare the magnitude of the random value R_2 and the security threshold ST to update the position of the Producers according to Equation (11). Update the Scroungers position according to the Equation (16) after introducing Lévy's flight strategy. Update the Perceivers position according to Equation (13);
- Step 5: According to the size of the current individual fitness value, perform Gaussian variation and tent chaos perturbation on the sparrow position after each iteration position update, and then one iteration is completed;
- Step 6: Updating individual fitness values f_i of sparrow populations, reorder the new population fitness to determine the current global optimal fitness value f_g and the global worst fitness value f_w and corresponding positions X_g and X_w;
- Step 7: Determine if the algorithm has reached the maximum number of iterations $Iter_{\max}$, and if the iterative maximum is reached, the optimal fitness value f_{best} of the sparrow population and its corresponding sparrow position X_{best} are output, where the optimal fitness value f_{best} is the objective solution of the requested optimal objective function, X_{best} is the set of optimal identification parameters sought. If not, go to step 4 and continue iteratively.

The flowchart of the ISSA is shown in Figure 5:

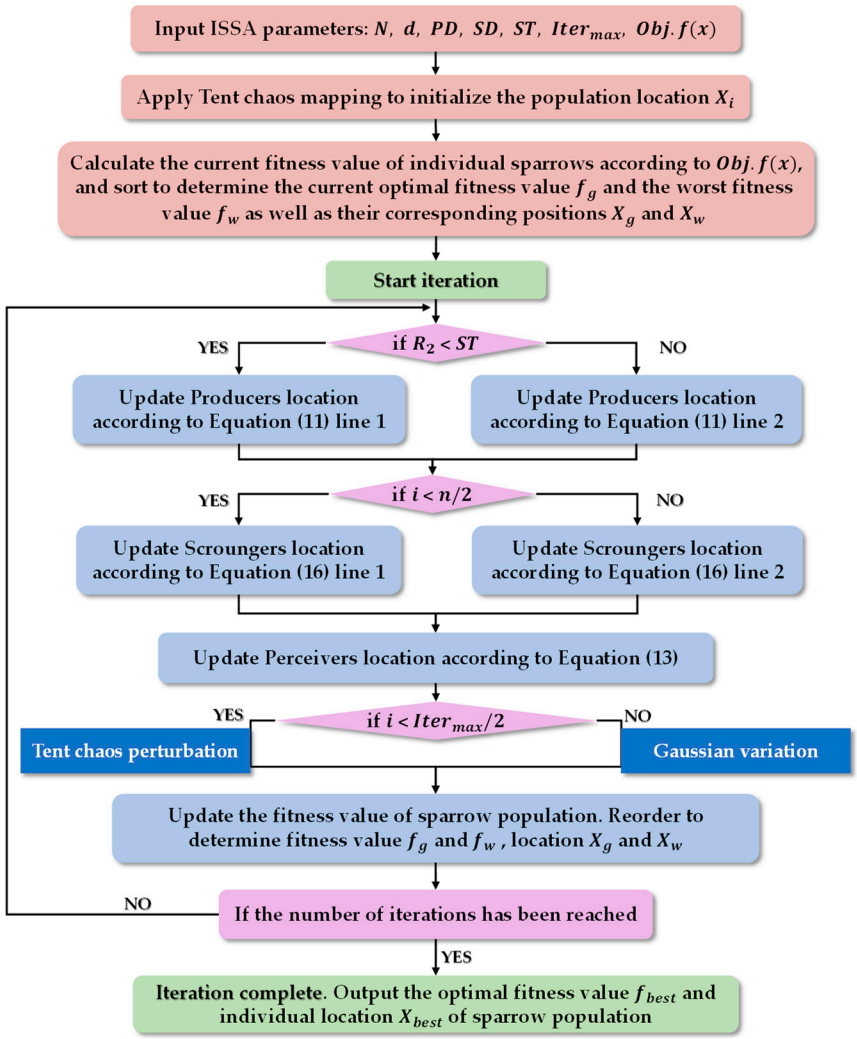

Figure 5. The flowchart of the ISSA.

4. Example Analysis of Parameter Identification

4.1. Data Acquisition

These research data come from the recording and broadcasting data of the PMU measurement device based on the Internet of things at the power grid side obtained by a traction substation in Tibet due to fault disturbance. The traction power supply method in this area adopts the direct power supply method with a return current line; the traction transformer type adopts three-phase V/v [30] wiring, and the locomotive is an HX_D1 [31] AC electric locomotive. The recording device installed in the substation records the instantaneous values of bus voltage and current before and after the substation disturbance to realize the input and output of parameter identification.

In the acquired recording data, the bus voltage perturbation causes the bus voltage to plunge by about 50%, and for the voltage perturbation curve for input data $U(k)$ and output data $P(k)$ and $Q(k)$, the data after normalization is shown in Figure 6 below:

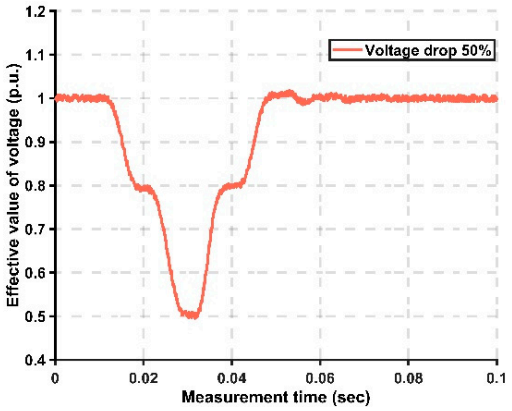

Figure 6. Measured voltage drop's 50% curve.

4.2. Parameter Identification

After obtaining the processed voltage input data, the ISSA is used to identify the parameters of the traction load. The flow chart of parameter identification is shown in Figure 7:

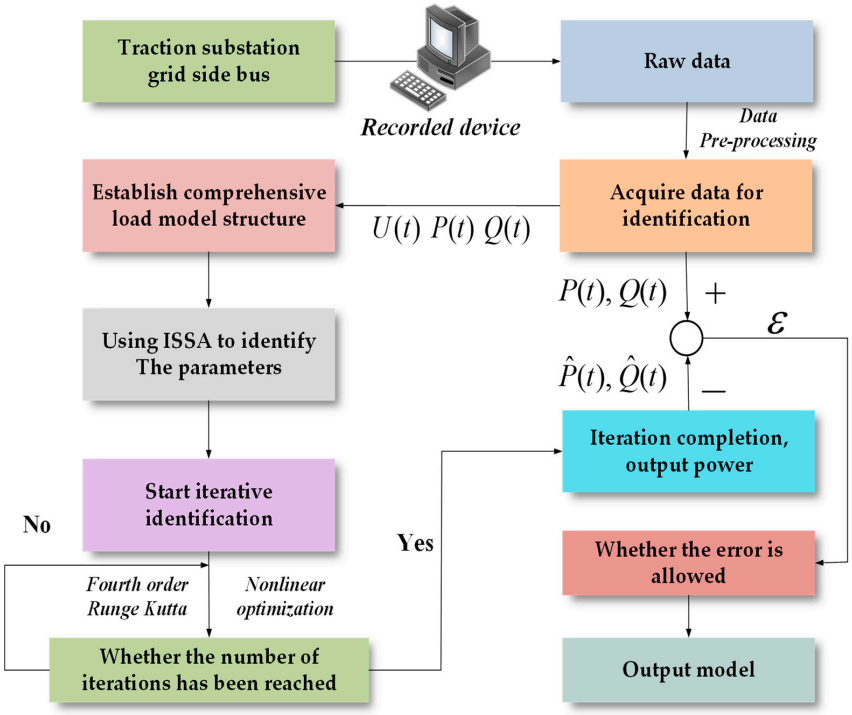

Figure 7. Schematic diagram of parameter identification process.

The ISSA identification algorithm is set as follows: sparrow population N = 50 (of which Producers account for 20% of the total population, Scroungers account for 80%, and 20% for Perceivers). The maximum number of iterations $Iter_{\max}$ is 300. For safety threshold $ST = 0.8$, the objective function (also the fitness value) is Equation (8): $Obj.E(\theta) = \frac{1}{N}\min \sum_{k=1}^{N} [(P_k - \hat{P}_k)^2 + (Q_k - \hat{Q}_k)^2]$.

After the algorithm is set, the parameters of the model are identified. The comparison of the active power and reactive power responses with the original data is shown in Figure 8:

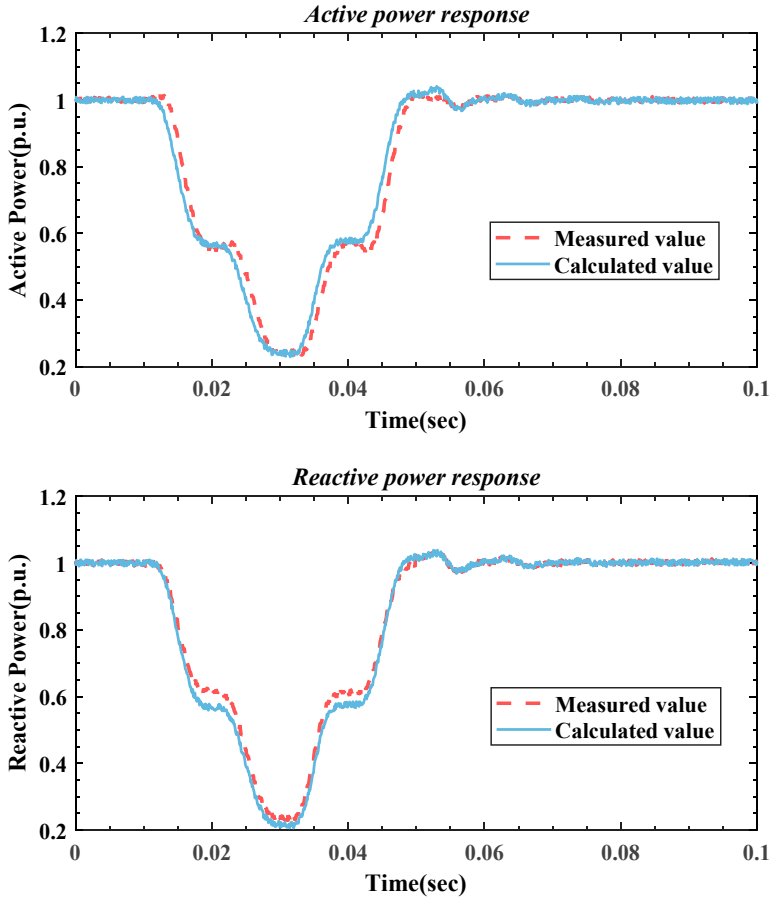

Figure 8. Fitting curve between measured data and calculated data.

Figure 8 shows that the output of the identified load model can accurately fit the measured power response curve, especially the reactive power.

According to the research in [7], the load model evaluation index can be evaluated by using the relative error coefficient:

$$\varepsilon = \frac{\left(\frac{1}{N}\sum_{k=1}^{N}[y(k) - \hat{y}(k)]^2\right)^{\frac{1}{2}}}{\left(\frac{1}{N}\sum_{k=1}^{N}[y(k)]^2\right)^{\frac{1}{2}}} \times 100\% \quad (20)$$

where $y(k)$ is the measured power, and $\hat{y}(k)$ is the calculated power (it can be active power or reactive power), and if the relative error is less than 5% [7], the load model is acceptable.

The results and errors of the parameters obtained after applying the ISSA to the identification of the model are shown in Table 2.

Table 2. Parameter identification values and errors.

Parameters	Identifying Value
T'	4.1354
X'	1.6654
C	−2.6241
M	0.82
T_m	3.378
p_v	3.5867
q_v	3.056
ε_p	3.847×10^{-2}
ε_q	6.07×10^{-3}
$Obj.E(\theta)$	2.851×10^{-3}

From Table 2, it can be seen that the identified parameters are all within reasonable ranges, the active and reactive errors are less than 5%, and the model is acceptable. The above results verify the effectiveness of the ISSA for the parameter identification of the composite load model.

4.3. Algorithm Comparison

In order to verify that the improved ISSA has the advantages of high accuracy and good convergence, the ISSA is compared with the SSA and PSO algorithms for experiments to jointly identify the parameters of this load model. The ISSA, SSA, and PSO algorithms are set as follows:

- ISSA: $N = 50$ ($PD = 10$, $SD = 20$), $ST = 0.8$, $Iter_{\max} = 300$;
- SSA: $N = 50$ ($PD = 10$, $SD = 20$), $ST = 0.8$, $Iter_{\max} = 300$;
- PSO: $N = 50$, $\omega = 0.8$, $c_1 = 0.5$, $c_2 = 1$, $Iter_{\max} = 300$.

After the algorithm is set up, the parameters of the load model are identified. The identification results and errors are shown in Table 3:

Table 3. Parameter identification values and errors for the three algorithms.

Parameters	ISSA	SSA	PSO
T'	4.1354	−3.8726	2.1863
X'	1.6654	1.8054	0.75606
C	−2.6241	1.8197	0.627
M	0.82	0.3427	1.7738
T_m	3.378	3.0239	1.2298
p_v	3.5867	1.9803	2.5629
q_v	3.056	2.128	1.286
ε_p	3.847×10^{-2}	4.4512×10^{-2}	4.1205×10^{-2}
ε_q	6.07×10^{-3}	1.135×10^{-2}	1.6175×10^{-2}
$Obj.E(\theta)$	2.851×10^{-3}	3.712×10^{-3}	4.49×10^{-3}

The global optimal fitness value reflects the change law of the global optimal solution in the iterative process of the algorithm and can reflect the convergence characteristics of the algorithm. Figure 8 takes the iteration times as the x-axis and the global optimal fitness value as the y-axis. The iterative change curves of the optimal fitness values of the three algorithms are shown in Figure 9:

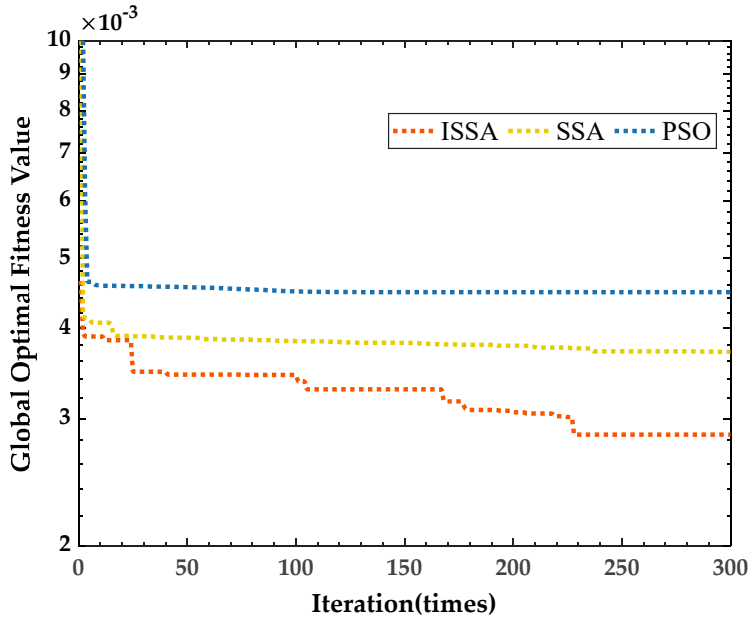

Figure 9. Fitness curves of ISSA, SSA, and PSO algorithms.

From Table 3 and Figure 9, it can be seen that:

- PSO: Although the accuracy and convergence speed of PSO is acceptable, it is easy to fall into local optimization. The values of the load model identified by PSO are acceptable, but the relative error of its active power is slightly higher;
- SSA: Although the search accuracy and convergence speed of the SSA are better than that of the PSO algorithm, it cannot jump out of the local optimal solution. The values of the load model identified by the SSA are acceptable, but the relative error of its active power is slightly higher;
- ISSA: After improvement, ISSA has the ability to search quickly and jump out of the local optimal solution, so its search accuracy and convergence speed are better than the SSA and PSO. Moreover, its active power response, especially reactive power response, is described more accurately.

Therefore, the ISSA has better accuracy and convergence than the SSA and PSO.

4.4. Model Generalization Capability Study

The generalization capability of a load model [32] refers to the ability of the model built using known data to interpret the load location change data, also known as interpolation extrapolation capability. A load model has real practical value only when it has good extrapolation and interpolation capabilities. This study evaluates the generalization ability of the load model from two aspects: load response fitting curve and response residual.

The response residual [33] can reflect the description ability of interpolation and extrapolation of the model and is one of the important indicators to evaluate the applicability of the model. The average value of the response residuals is as follows:

$$\hat{\varepsilon} = \frac{1}{N}\sum_{k=1}^{N}\left(\left|X_k - \hat{Y}_k\right|\right) \tag{21}$$

where X is the calculated power data of the original response of the model itself, and $\hat{Y}$ is the actual power data of the interpolation or extrapolation response.

4.4.1. Interpolation Capability

Through the recording and broadcasting device, the disturbance data with a voltage disturbance of less than 50% is obtained, and the load model in Table 2 identified by ISSA is tested to verify the interpolation ability of the model. The results are shown in Figure 10:

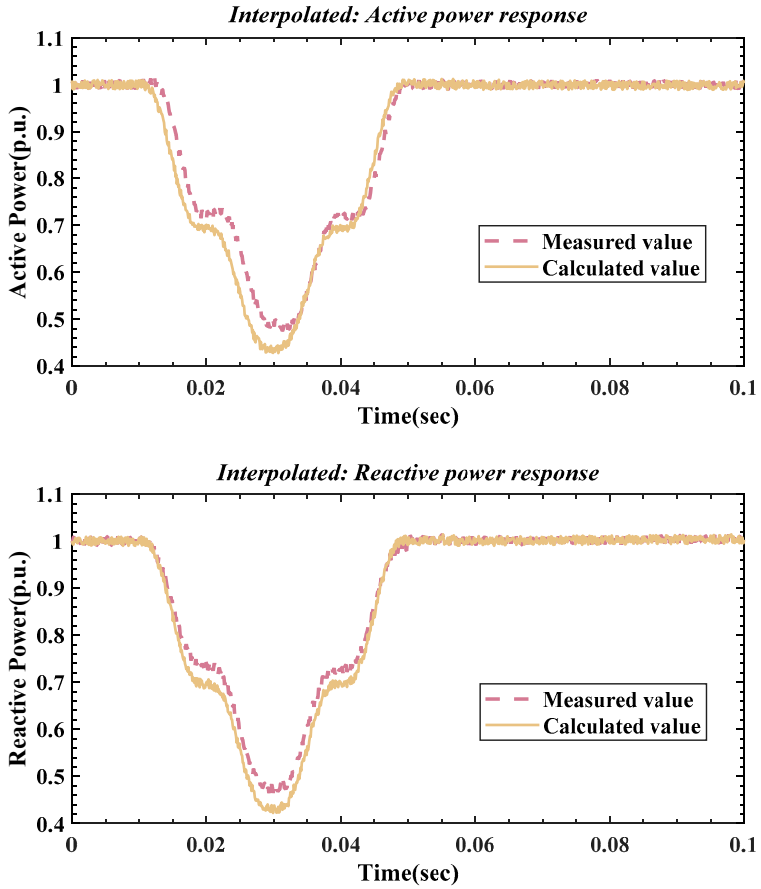

Figure 10. Interpolation fitting curve between measured data and calculated data.

It can be seen from Figure 10 that although there is some error between the interpolation response value calculated by the model and the change curve of the measured value, the response tracking fitting curve is basically consistent, which indicates that the model has good nonlinear interpolation ability.

This study compares the interpolation ability of the models identified by the SSA and PSO algorithms by calculating the values of the response residuals. The mean values of residuals for each algorithm are shown in Table 4.

Table 4. Interpolation response residual.

Algorithm	Active Power Interpolation Residual	Reactive Power Interpolation Residual
ISSA	1.66×10^{-2}	2.987×10^{-3}
SSA	1.81×10^{-2}	7.46×10^{-3}
PSO	1.48×10^{-2}	6.1×10^{-3}

From Table 4, it can be seen that the models identified by different algorithms have different interpolation capabilities for active and reactive power descriptions, and the overall model identified by the ISSA has a better interpolation capability, especially the reactive power interpolation response.

4.4.2. Extrapolation Capability

Through the recording and broadcasting device, the disturbance data with a voltage disturbance of less than 50% is obtained, and the load model in Table 2 identified by the ISSA is tested to verify the extrapolation ability of the model. The results are shown in Figure 11:

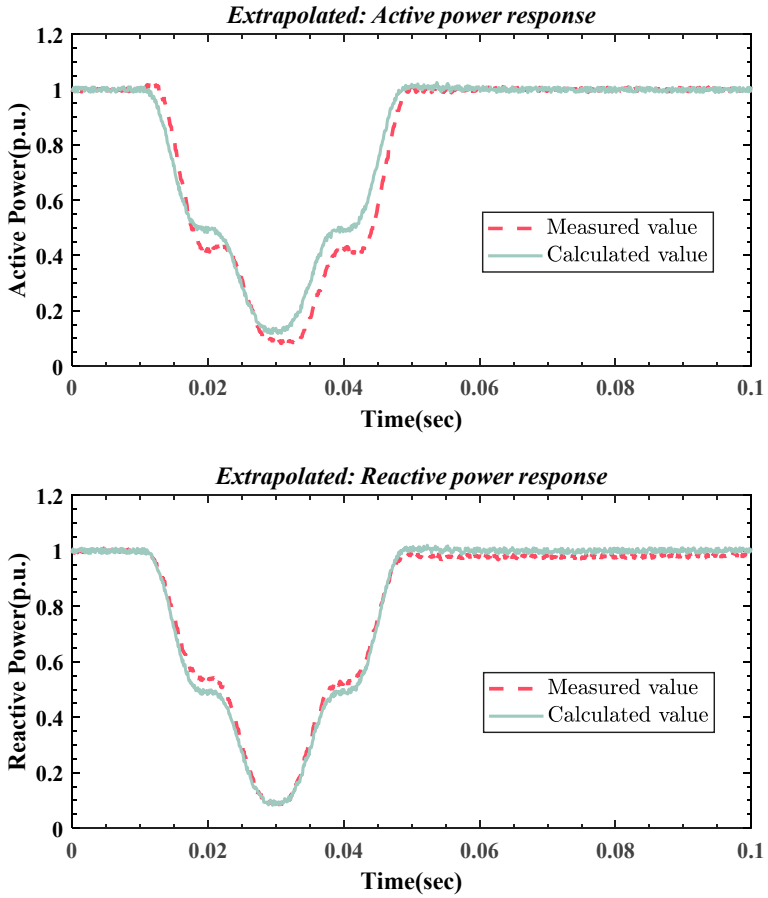

Figure 11. Extrapolation fitting curve of measured data and calculated data.

It can be seen from Figure 11 that although there is some error between the extrapolation response value calculated by the model and the change curve of the measured value, the response tracking fitting curve is basically consistent, which indicates that the model has good nonlinear extrapolation ability.

From Table 5, it can be seen that the models identified by different algorithms have different extrapolation capabilities for active and reactive power descriptions, and the overall model identified by the ISSA has a better interpolation capability.

Table 5. Extrapolation response residual.

Algorithm	Active Power Extrapolation Residual	Reactive Power Extrapolation Residual
ISSA	2.86×10^{-2}	1.3×10^{-2}
SSA	3.11×10^{-2}	2.31×10^{-2}
PSO	2.76×10^{-2}	2.11×10^{-2}

In general, the models identified by the ISSA have relatively better generalization capabilities, including interpolation and extrapolation capabilities, than those identified by the SSA and PSO.

5. Conclusions

In this paper, an improved sparrow search algorithm, ISSA, is proposed and applied to the parameter identification of the traction-integrated load model. The following conclusions are obtained through the application of algorithm identification analysis:

1. The load disturbance data are obtained from the recording and broadcasting data, a suitable traction load model is established, and its parameters are identified by the ISSA. The identification results meet the relative error of the dynamic load model, which verifies the correctness and effectiveness of the ISSA applied to the parameter identification of the comprehensive load model;
2. The results show that compared with the other two algorithms, the ISSA has stronger ergodicity in searching individuals and better performance in convergence speed and accuracy, as well as being able to constantly jump out of local optima;
3. The generalization ability of the identified load model was studied. The results show that the load model identified by the ISSA has good interpolation and extrapolation ability. Therefore, the ISSA can improve the accuracy of load modeling and show practical value.

Since the balance degree of negative sequence voltage on the 220 kV power grid side is considerable, this paper does not consider too much the negative sequence current and harmonic in the research, and future work should analyze and model these two aspects.

Author Contributions: Conceptualization, D.F. and Z.W.; methodology, D.F.; software, D.F.; validation, D.F. and Z.W.; formal analysis, Z.W.; writing—original draft preparation, D.F. and F.Z.; writing—review and editing, D.F. and F.Z; supervision, Z.W. All authors have read and agreed to the published version of the manuscript.

Funding: This research was funded by the National Key Research and Development Program of China under grant 2018YFB2100100.

Institutional Review Board Statement: Not applicable.

Informed Consent Statement: Not applicable.

Data Availability Statement: Not applicable.

Conflicts of Interest: The authors declare no conflict of interest.

References

1. Ma, J.; Han, D.; He, R.-M.; Dong, Z.-Y.; Hill, D.J. Reducing identified parameters of measurement-based composite load model. *IEEE Trans. Power Syst.* **2008**, *23*, 76–83. [CrossRef]
2. Kessel, P.; Glavitsch, H. Estimating the Voltage Stability of a Power-System. *IEEE Trans. Power Deliv.* **1986**, *1*, 346–354. [CrossRef]
3. Price, W.W.; Chiang, H.D.; Clark, H.K.; Concordia, C.; Lee, D.C.; Hsu, J.C.; Ihara, S.; King, C.A.; Lin, C.J.; Mansour, Y.; et al. Load Representation for Dynamic Performance Analysis. *IEEE Trans. Power Syst.* **1993**, *8*, 472–482.
4. Price, W.W.; Wirgau, K.A.; Murdoch, A.; Mitsche, J.V.; Vaahedi, E.; Elkady, M.A. Load Modeling for Power Flow and Transient Stability Computer Studies. *IEEE Trans. Power Syst.* **1988**, *3*, 180–187. [CrossRef]
5. Lin, C.J.; Chen, Y.T.; Chiou, C.Y.; Huang, C.H.; Chiang, H.D.; Wang, J.C.; Fekihahmed, L. Dynamic Load Models in Power-Systems Using the Measurement Approach. *IEEE Trans. Power Syst.* **1993**, *8*, 309–315. [CrossRef]
6. Ju, P.; Liu, W.; Xiang, L.; Yu, Y.; Ding, M.; Chen, Q. Automatic post-disturbance simulation based method for power system load modeling. *Dianli Xitong Zidonghua/Autom. Electr. Power Syst.* **2013**, *37*, 60–64.
7. Choi, B.K.; Chiang, H.D.; Li, Y.H.; Li, H.; Chen, Y.T.; Huang, D.H.; Lauby, M.G. Measurement-based dynamic load models: Derivation, comparison, and validation. *IEEE Trans. Power Syst.* **2006**, *21*, 1276–1283. [CrossRef]
8. Li, H.Q.; Jiang, J.H.; Mohamed, M.S. Online Dynamic Load Identification Based on Extended Kalman Filter for Structures with Varying Parameters. *Symmetry* **2021**, *13*, 1372. [CrossRef]
9. Ju, P.; Handschin, E. Identifiability of load models. *IEE Proc. Gener. Transm. Distrib.* **1997**, *144*, 45–49. [CrossRef]
10. Bai, H.; Zhang, P.; Ajjarapu, V. A Novel Parameter Identification Approach via Hybrid Learning for Aggregate Load Modeling. *IEEE Trans. Power Syst.* **2009**, *24*, 1145–1154. [CrossRef]
11. Wang, Z.; Bian, S.; Liu, X.; Yu, K.; Shi, Y. Research on load model parameter identification based on the CQDPSO algorithm. *Diangong Jishu Xuebao/Trans. China Electrotech. Soc.* **2014**, *29*, 211–217.
12. Mirjalili, S. Dragonfly algorithm: A new meta-heuristic optimization technique for solving single-objective, discrete, and multi-objective problems. *Neural Comput. Appl.* **2016**, *27*, 1053–1073. [CrossRef]

13. Mirjalili, S.; Lewis, A. The Whale Optimization Algorithm. *Adv. Eng. Softw.* **2016**, *95*, 51–67. [CrossRef]
14. Saremi, S.; Mirjalili, S.; Lewis, A. Grasshopper Optimisation Algorithm: Theory and application. *Adv. Eng. Softw.* **2017**, *105*, 30–47. [CrossRef]
15. Yang, X.S. A New Metaheuristic Bat-Inspired Algorithm. In Proceedings of the International Workshop on Nature Inspired Cooperative Strategies for Optimization (NICSO 2008), Tenerife, Spain, 12–14 November 2008; pp. 65–74.
16. Xue, J.K.; Shen, B. A novel swarm intelligence optimization approach: Sparrow search algorithm. *Syst. Sci. Control. Eng.* **2020**, *8*, 22–34. [CrossRef]
17. Yali, L.; Shuqin, W.; Qianru, C.; Xiaogang, W. Comparative Study of Several New Swarm Intelligence Optimization Algorithms. *Comput. Eng. Applications.* **2020**, *56*, 1–12.
18. Zhu, Y.; Yousefi, N. Optimal parameter identification of PEMFC stacks using Adaptive Sparrow Search Algorithm. *Int. J. Hydrogen Energy* **2021**, *46*, 9541–9552. [CrossRef]
19. Hairui, W.; Jianchuan, X. Application of Distributed Generation Configuration Based on Improved Sparrow Search Algorithm. *Jisuanji Gongcheng Yu Yingyong/Comput. Eng. Appl.* **2021**, *57*, 245–252.
20. Yuan, J.; Zhao, Z.; Liu, Y.; He, B.; Wang, L.; Xie, B.; Gao, Y. DMPPT Control of Photovoltaic Microgrid Based on Improved Sparrow Search Algorithm. *IEEE Access* **2021**, *9*, 16623–16629. [CrossRef]
21. Liu, G.; Shu, C.; Liang, Z.; Peng, B.; Cheng, L. A modified sparrow search algorithm with application in 3d route planning for uav. *Sensors* **2021**, *21*, 1224. [CrossRef]
22. Li, X.J.; Gu, J.A.; Sun, X.H.; Li, J.; Tang, S.X. Parameter identification of robot manipulators with unknown payloads using an improved chaotic sparrow search algorithm. *Appl. Intell.* **2022**, *52*, 10341–10351. [CrossRef]
23. Choi, B.-K.; Chiang, H.-D.; Li, Y.; Chen, Y.-T.; Huang, D.-H.; Lauby, M.G. Development of Composite Load Models of Power Systems using On-line Measurement Data. *J. Electr. Eng. Technol.* **2006**, *1*, 161–169. [CrossRef]
24. Choi, B.K.; Chiang, H.D. Multiple Solutions and Plateau Phenomenon in Measurement-Based Load Model Development: Issues and Suggestions. *IEEE Trans. Power Syst.* **2009**, *24*, 824–831. [CrossRef]
25. Rudion, K.; Guo, H.; Abildgaard, H.; Styczynski, Z.A. Non-linear load modeling—Requirements and preparation for measurement. In Proceedings of the 2009 IEEE Power and Energy Society General Meeting, PES '09, Calgary, AB, Canada, 26–30 July 2009; IEEE Computer Society: Washington, DC, USA, 2009.
26. Ahmedzaid, S.; Taleb, M. Structural Modeling of Small and Large Induction Machines Using Integral Manifolds. *IEEE Trans. Energy Convers.* **1991**, *6*, 529–535. [CrossRef]
27. Li, C.H.; Luo, G.C.; Qin, K.; Li, C.B. An image encryption scheme based on chaotic tent map. *Nonlinear Dyn.* **2017**, *87*, 127–133. [CrossRef]
28. Qin, H.L.J.E.M. Control, A chaotic search method for global optimization on tent map. *Mach. Control.* **2004**, *8*, 67–70.
29. Mantegna, R.N.; Stanley, H.E. Stochastic-Process with Ultraslow Convergence to a Gaussian—The Truncated Levy Flight. *Phys. Rev. Lett.* **1994**, *73*, 2946–2949. [CrossRef]
30. Chu, Z.-Y.; Wu, M.-L.; Zhang, J.; Lin, Z.-L. Combined application of three-phase V, v connection and single-phase I, i connection traction transformer. *Tiedao Xuebao/J. China Railw. Soc.* **2007**, *29*, 109–114.
31. Xu, Z.; Li, Q.; Fu, C.; Li, Y.; Liao, H. HXD1 high-power heavy-duty electric freight locomotive. In Proceedings of the 9th International Heavy Haul Association Conference: Heavy Haul and Innovation Development, IHHA 2009, Shanghai, China, 22–25 June 2009; International Heavy Haul Association: Shanghai, China, 2009; pp. 581–593.
32. Ren-Mu, H.; Germond, A.J. Comparison of dynamic load modeling using neural network and traditional method. In Proceedings of the 2nd International Forum on Applications of Neural Networks to Power Systems, ANNPS 1993, Yokohama, Japan, 19–22 April 1993; Institute of Electrical and Electronics Engineers Inc.: Yokohama, Japan, 1993; pp. 253–258.
33. Zheng, X.; Ma, J.; He, R.; Tang, Y.J. Classification and Generalization of the Load Model Based on Model Dynamic Responses. *Trans. China Electrotech. Soc.* **2009**, *24*, 132–138.